

Microwave excitations associated with a wavy angular dependence of the spin transfer torque : model and experiments

O. Boulle,^{*} V. Cros,[†] J. Grollier, L.G. Pereira,[‡] C. Deranlot, F. Petroff, and A. Fert

Unité mixte de physique CNRS/Thales and Université Paris Sud-11,

Route départementale 128, 91767 Palaiseau, France

G. Faini

Phynano team, Laboratoire de Photonique et de Nanostructures LPN-CNRS,

Route de Nozay, 91460 Marcoussis, France

J. Barnaś

Department of Physics, Adam Mickiewicz University,

Umultowska 85, 61-614 Poznan, Poland

(Dated: February 9, 2022)

Abstract

The spin transfer torque (STT) can lead to steady precession of magnetization without any external applied field in magnetic spin valve where the magnetic layer have very different spin diffusion length. This effect is associated with an unusual angular dependence of the STT, called "wavy" (WAD-STT), predicted in the frame of diffusive models of spin transfer. In this article, we present a complete experimental characterization of the magnetization dynamics in the presence of a WAD-STT. The results are compared to the prediction of the magnetization dynamics obtained by single domain magnetic simulations (macrospin approximation). The macrospin simulations well reproduced the main static and dynamical experimental features (phase diagram, R(I) curves, dependence of frequency with current and field) and suggest that the dynamical excitations observed experimentally are associated with a large angle out-of-plane precession mode. The present work validates the diffusive models of the spin transfer and underlines the role of the spin accumulation and the spin relaxation effects on the STT.

^{*}Present adress: Universität Konstanz, Universitätsstr. 10, D - 78457 Konstanz, Germany :
olivier.boulle@uni-konstanz.de

†Corresponding author : vincent.cros@thalesgroup.com

‡Present adress: Instituto de Fisica, UFRGS, 91501-970 Porto Alegre, RS, Brazil

1. INTRODUCTION

A spin polarized current can exert a torque on the magnetization of a ferromagnetic body, via transfer of spin angular momentum. This spin transfer effect, originally introduced by J.Slonczewski and L.Berger^{1,2}, has opened a new route to manipulate a magnetization using an electrical current. Today, it is the subject of extensive experimental and theoretical research motivated not only by its fundamental interest but also by promising applications in the field of magnetic memories and microwave devices for future telecommunication systems. In most experiments, this effect has been studied in pillar shaped F1/NM/F2 trilayers in which a magnetic layer F1 with a fixed magnetization is used to prepare a spin polarized current injected in a magnetically free magnetic layer F2. When the spin polarized current enters the free layer, the part of the spin current that is non-collinear to the magnetization of the free layer is absorbed and transferred to the local magnetization; this spin transfer is equivalent to a torque exerted on magnetization. In *standard* structures such as Co/Cu/Co or NiFe/Cu/NiFe, at zero or low applied field, the spin transfer torque (STT) leads to an irreversible switching of the magnetization from one static configuration to another one^{3,4} (so called CIMS effect). For larger fields (typically higher than the coercive field of the free layer), the spin transfer torque compensates for the damping torque resulting in a steady precession of magnetization around the local internal field. Owing to the giant magnetoresistance (GMR) effect, this high frequency magnetization precession goes with voltage oscillations in the microwave range^{5,6}. These two behaviors (magnetization switching and precession) open two branches of potential technological applications of the spin transfer effect: first, a new and more reliable way to write the magnetic bit in magnetic memories and second, a new type of sub-micrometric microwave oscillators for future telecommunication devices combining high quality factor and large frequency agility with current and field ⁶.

Following the original approach of Slonczewski¹, several theoretical studies underlined that the STT is directly related to the spin polarization of the spin current entering the magnetic free layer and more precisely to the absorption of the spin current's component transverse to the magnetization^{7,8}. In the first generation of spin transfer models^{1,2,9}, this spin polarization was calculated in a ballistic assumption. The magnetic multilayer is contacted to reservoirs with uniform chemical potentials and the spin polarization of the current arises from the spin dependent reflections at the interfaces of the multilayer and from spin

dependent scattering inside the magnetic layers. However, since the study of the CPP-GMR^{10,11}, it is well known that, in this geometry, the spin polarization of the current is strongly affected by the spin accumulation which is controlled by spin relaxation effects in the whole structure. To correctly describe the electronic transport, diffusive models that also take into account this relaxation must be considered¹⁰. Indeed recent spin transfer models do take into account these diffusive transport aspects^{7,8,12,13,14,15}.

The first experimental evidence of diffusive effects on the STT was given by Urazhdin *et al.*¹⁶ and Alhajdarwish *et al.*¹⁷. They demonstrated the influence of the *spin dependent scattering* by magnetic impurities on the STT features in the CIMS regime at low magnetic field : by doping the polarizing layer with impurities, the amplitude and even the sign of the torque was changed. More recently, we demonstrated experimentally the influence of the *spin relaxation effect* on the STT¹⁸. We showed that by acting on the distribution of spin relaxation in the structure through different spin diffusion lengths in the two magnetic layers, the STT and thus the dynamics of magnetization induced by this torque can be strongly modified compared to *standard* structures. This was made by studying the magnetization dynamics induced by the STT in a Co(8 nm)/Cu/Py(8 nm) (Py=Ni₈₀Fe₂₀) nanopillar through both static and high frequency magneto-transport measurements. In such a structure, an unusual dependence of the STT with the angle φ between both magnetization is predicted in the frame of diffusive models of spin transfer^{13,19,20} (see Fig. 1). This so called Wavy Angular Dependence of the Spin Transfer Torque (WAD-STT) arises from the modification of the spin accumulation profile in the structure caused by the different ratios *thickness / spin diffusion length* of the magnetic layers. It is characterized by a change of sign of the STT between 0 (parallel configuration (*P*)) and π (antiparallel configuration (*AP*)). This angular dependence modifies the stability of the static states *P* and *AP*: for one polarity of the current (negative current in our convention), both states are stabilized by the STT whereas they are destabilized for the opposite polarity (positive current). In the latter case, it is predicted that the magnetization precesses even at zero external magnetic field. These predictions were validated experimentally by the present authors by measuring the microwave emission caused by the steady precession of magnetization induced by the STT at zero (or low) applied field¹⁸.

In this manuscript, we present a complete characterization and analysis of the magnetization dynamics in the presence of a WAD-STT. The results are compared to the prediction

of the magnetization dynamics obtained by single domain magnetic simulations (macrospin approximation). We show that the main static and dynamical experimental features such as current-field phase diagram, variation of resistance with current, variation of frequency with current and field can be reproduced by simulation, at least qualitatively and for some features quantitatively. Therefore, the present work validates the diffusive models of the spin transfer^{7,8,12,21}.

The paper is organized as follows. We first described the predictions of the macrospin simulations taking into account the WAD-STT. In a second section, we present the results of low field static and high frequency measurements obtained on a Co(8 nm)/Cu/Py(8 nm) nanopillar in which a WAD-STT is predicted. These results are compared with the predictions of the macrospin simulations and discussed in a third part .

2. MACROSPIN SIMULATIONS WITH A WAVY ANGULAR DEPENDANCE OF THE SPIN TRANSFER TORQUE (WAD-STT)

2.1. Method

In this section, we present the results of the simulations for the magnetization dynamics of the Py free layer of a Co(8 nm)/Cu/Py(8 nm) trilayer, on the basis of the predicted *wavy* angular dependence of the torque (labelled as WAD-STT). These calculations have been carried out in the macrospin approximation, *i.e* by assuming the magnetization to be uniform during its motion. The magnetization of the Py free layer is described by a unit vector $\vec{m} = m_x\vec{u}_x + m_y\vec{u}_y + m_z\vec{u}_z$ and makes an angle φ with the magnetization of the Co layer which is supposed fixed and aligned along the x axis. As in experiments, the Py free layer has got an elliptical shape of dimensions 100x155 nm² and a thickness t_{Py} of 8 nm. This results in an in-plane uniaxial anisotropy field $\vec{H}_{an} = H_{an}m_x\vec{u}_x$ aligned along the direction of the long axis \vec{u}_x of the ellipse and a demagnetizing field $\vec{H}_d = -H_d m_z\vec{u}_z$, with \vec{u}_z perpendicular to the plane of the layer. The external field $\vec{H}_{app} = H_{app}\vec{u}_x$ is applied in the plane of the layer and aligned along the direction \vec{u}_x of the uniaxial anisotropy field. The time dependent trajectory $\vec{m}(t)$ is found by solving the modified Landau-Lifschitz-Gilbert (LLG) equation including the STT $\vec{\tau}$:

$$\frac{d\vec{m}}{dt} = -\gamma_0 \vec{m} \times \vec{H}_f + \alpha \vec{m} \times \frac{d\vec{m}}{dt} - \frac{\gamma_0}{\mu_0 M_s V} \vec{\tau} \quad (1)$$

Here γ_0 is the absolute value of the gyromagnetic ratio, α the parameter of the Gilbert damping, M_s the saturation magnetization, V the volume of the Py nanomagnet and \vec{H}_f an effective field which includes \vec{H}_{app} , \vec{H}_{an} and \vec{H}_d . In order to characterize the influence of thermal activation on the magnetization dynamics, the simulations were carried out both at $T=0$ K and $T=300$ K. Thermal effects are simulated by introducing a randomly fluctuating field \vec{H}_T ^{22,23} with $\mu_0\vec{H}_T = \sqrt{2k_B T \alpha / V M_s \gamma \Delta t} \vec{H}_{al}$, where \vec{H}_{al} is a random gaussian field with $\langle \vec{H}_{al} \rangle = 0$ and $\langle H_{al}^2 \rangle = 1$, k_B is the Boltzmann's constant and Δt the integration step. The magnetic parameters used for the simulations are described in appendix A with computational details. The spin transfer term is defined as $\vec{\tau} = P(\varphi) \frac{I\hbar}{2e} \vec{m} \times \vec{m} \times \vec{u}_x$, I is the current (defined as positive when the electrons flow from the fixed Co layer to the Py free layer), e is the absolute value of the electron charge. The polarization factor $P(\varphi)$ is derived from the angular dependence of the torque calculated from the Barnas-Fert model (see Fig. 1).

The displayed phase diagrams are constructed by calculating the mean values over the integration time of $\sigma_{mx} = \sqrt{\langle m_x^2 - \langle m_x \rangle^2 \rangle}$ after relaxation (σ_{mx} gives an evaluation of the amplitude of precession). These two quantities allow to determine the borders between the different static and dynamical states. All presented simulations have been carried out for a positive current. No excitations are predicted by the simulations for a negative current⁴¹.

2.2. Results

2.2.1. $T=0$ K

In Fig. 2(a) and (b), we show respectively the variation of the frequency and the resistance as a function of the current for zero applied field (black curves). Starting from an initial P configuration and increasing current (plain line), the magnetization goes into sustained precession around the in plane effective field (in plane precession mode IP_P) for a threshold current I_c^1 (black point at $I=4.8$ mA) with a precession frequency ($f=2.28$ GHz) close to the Kittel's frequency of the FMR small angles precession ($f=2.23$ GHz). When the current is increased above I_c^1 , the angle of precession increases but the frequency decreases ("red shift regime"). This behavior, i.e. the decrease of frequency with increasing current is a nonlinear effect due to the dependence of the frequency on the precession amplitude^{24,25,26}. In this

mode, only a small increase of the resistance with increasing current is predicted, although a large angle precession can be reached. For a threshold current I_c^{2+} (orange point at $I=12$ mA), the magnetization dynamics changes abruptly to an out-of-plane precession mode (labelled as OP_P). This transition is associated with a jump in frequency and a large increase of the resistance. In this OP_P regime, the magnetization precesses around the demagnetizing field and the frequency is set by the mean out-of-plane component of magnetization $\langle m_z \rangle$. For increasing current, the trajectory goes away from the plane of the layer (higher $\langle m_z \rangle$) and the frequency increases ("blue shift regime"). For higher current ($I > 13$ mA, not shown), the magnetization precesses faster (up to 20 GHz) around circular trajectories of decreasing radius while current is increased. These trajectories converge for even higher current to a quasi-static out-of-plane state OP_S . As shown in Fig. 2(a-b), the transition between the IP_P and the OP_P precession modes is irreversible): the critical current for this transition is higher for increasing current (I_c^{2+} , orange point and plain line) than for decreasing current (I_c^{2-} , blue point and dashed line), which results in hysteretic $R(I)$ and $f(I)$ curves.

In addition, we display in Fig. 2(a) the variation of the frequency as a function of the current for a higher negative applied field $H = -20$ Oe (red curve). In the IP_P mode, the black curve ($H=0$ Oe) is above the red curve ($H=-20$ Oe): the frequency increases with field. On the contrary, in the OP_P mode, the black curve is below the red curve and the frequency decreases with field: the in-plane field pulls magnetization in the plane of the layer, decreasing $\langle m_z \rangle$ and therefore the frequency.

We present in Fig. 2(c) a calculated current-field dynamical phase diagram for increasing current starting from an initial P configuration. The amplitude of precession (σ_{mx}) is plotted in a color scale. Several regimes can be defined. First, at high positive field ($H > +25$ Oe) (see the orange dashed line in Fig. 2(c)), only the IP_P mode is observed for $I_c^1 < I < I_c^3$. For $I > I_c^3$, the magnetization goes into the quasi-static out-of-plane precession state OP_S . In a second regime at low field i.e. for fields smaller than the coercive field (see the white dotted line on Fig. 2(c)), the out-of-plane precession mode OP_P appears for I above I_c^{2+} with $I_c^1 < I_c^{2+} < I < I_c^3$. The amplitude of precession (red color) and therefore the emitted power is maximum in this mode. The aforementioned hysteretic behavior appears also on the phase diagram: the OP_P/IP_P frontier is not the same for *increasing* current (colored frontier, I_c^{2+}) and *decreasing current* (dashed lines, I_c^{2-}). At higher current and field ($H > +25$ Oe), the transition to the OP_S state is also irreversible: for increasing current (colored frontiers),

magnetization switches from IP_P to OP_S and for decreasing current from OP_S to OP_P (dotted lines).

Finally, for even a lower applied field ($H < -50$ Oe), before reaching the OP_P mode, the magnetization first precesses in-plane around the AP state (mode denoted as IP_{AP}). Note that in this mode, the frequency increases with current and decreases with (positive) field. Starting from an initial AP state ($H < -90$ Oe), this precession state IP_{AP} is the first observed when current is increased from zero.

To summarize, the magnetization dynamics in a WAD-STT structure is very different from what is predicted for a *standard* angular dependence structure:

- For $H > H_c$, where H_c is the coercive field of the free layer, the precession modes are predicted for a positive current for a WAD-STT structure in our current convention, whereas they are obtained for a negative current for a *standard* structure.
- For $H < H_c$, in the *standard* case, only small angle IP_P precessions around the in-plane effective field are predicted in a very narrow range of current before the magnetization switches to the other stable static state (P or AP) due to the increase of the precession amplitude with current^{27,28}. In the case of a WAD-STT, both static states (P or AP) are unstable and this in-plane-precession mode is present on a much larger range of current. In a similar manner to what is observed for a standard angular dependence at high field, large angle in-plane trajectories bifurcate into out-of-plane trajectories at higher current^{26,28}. One can note that this large angle out-of-plane precession is predicted even in the absence of any external field. It is therefore possible in this structure to emit microwaves at zero field, only by injecting a current in the structure.

2.2.2. $T=300$ K

The main effect of temperature is the almost complete disappearance of the irreversibility associated with the transition from the IP_P to the OP_P precession mode. The thermal energy allows the magnetization to go across the energy barrier that separates these two states. This appears on the phase diagram of Fig. 3(c): the frontiers between the two states are quasi-identical for increasing (colored frontier) or decreasing current (dashed lines), except at large applied field ($H > 60$ Oe). As a consequence, this reversible behavior leads to an

expansion of the current-field region in which the OP_P precession mode occurs: for a given value of the applied field, the critical current for the transition from IP_P to OP_P is lower at $T=300$ K⁴². The reversibility of this transition results in non-hysteretic $f(I)$ and $R(I)$ curves as shown in Fig. 3(a-b))⁴³. The effect of thermal energy appears in particular in the transition zone between the two states and especially for currents close to the minimum in frequency ($I \approx 9.1$ mA). In this zone, the thermal energy makes the system unstable and telegraph noise with a characteristic time of about 10 ns is observed between the state IP_P and the two degenerated out-of-plane trajectories which are symmetrical around the (xy) plane. To conclude this section, the temperature does not modify the main characteristics of the dynamics in a WAD-STT structure, such as a steady precession at zero applied field.

3. EXPERIMENTAL RESULTS AND COMPARISON WITH MACROSPIN SIMULATIONS

We present a detailed experimental characterization of the magnetization dynamics induced by STT on a Co(8 nm)/Cu(10 nm)/Py(8 nm) nanopillar in which a WAD-STT is predicted. This dynamics was studied by measurements of the high frequency voltage oscillations generated by the magnetization precession with a spectrum analyzer after amplification. To directly compare the experimental results with simulations, we consider for experiments an effective external field H_{eff} that takes into account the contribution from the dipolar field exerted on the Py free layer ($H_{dip} \approx -43$ Oe).

3.1. Initial configuration : P

In Fig. 4(a), we display the microwave spectra measured for several values of injected current and a fixed effective applied field $H_{eff} = -62$ Oe . The corresponding variation of the frequency with current at this field is plotted in Fig. 4(b). The analysis of the frequency dependence with current allows the definition of three different dynamical regimes. At low current ($4 \text{ mA} \leq I \leq 9 \text{ mA}$), we observe that the frequency increases with current i.e. a blue shift with current (regime 1). Then it stays approximately constant for $9 \text{ mA} \leq I \leq 10 \text{ mA}$ (regime 2). At higher current ($I > 10 \text{ mA}$), a slight decrease of frequency with current is observed, i.e. a red shift with current (regime 3)⁴⁴. Three corresponding

behaviors are observed in the frequency dependence with field as illustrated in Fig. 4(c) by the microwave spectra measured for a constant current of 10 mA and several values of applied field. The corresponding frequency are plotted Fig. 4(d)). In the low field range ($-47 \text{ Oe} \leq H_{eff} \leq 2 \text{ Oe}$), the frequency decreases with field (regime 1). At higher negative field ($-62 \text{ Oe} \leq H_{eff} \leq -47 \text{ Oe}$), the frequency remains approximately constant ($f \approx 3.5 \text{ GHz}$) with field (regime 2). Then in a narrow experimental window for H_{eff} very close to the switching field, the frequency decreases with field (regime 3).

In Fig. 4(e), we present a current-field dynamical phase with the microwave power plotted in color scale. As predicted by the model, the microwave power is emitted for a *positive* current and at low field ($H_{eff} < 30 \text{ Oe}$), i.e smaller than the coercive field, and in particular at *zero effective field*. This behaviour is very different from the one typically observed in standard structures, where steady precession associated with microwave emission is observed at *high field*, i.e higher than the coercive field, and for a *negative* current^{5,29}. In addition, we plot on the diagram in plain lines the frontiers between the different dynamical regimes presented above⁴⁵. In regime 1, the frequency increases with current and decreases with field. It is present in the largest part of the region of the phase diagram where a power emission is observed. This behaviour is indeed the only one observed at low current (from $I \geq 4 \text{ mA}$) and close to zero effective field. The regime 2 appears at low applied field and for higher currents. It is characterized by a frequency that remains approximately constant with the current and also with the applied field. Finally, the regime 3 in which the frequency slightly decreases with current (and increases with field) is observed in the top-left corner of the diagram corresponding to large current and applied fields close to the switching field ($H_{eff} \approx -90 \text{ Oe}$).

We can directly compare the experimental results to the simulated dynamical phase diagram shown in Fig. 4(f). The current-field region in which an out-of-plane precession OP_P mode is predicted (red color in Fig. 4(e)) coincides with the zone in which the high frequency power is measured (dynamical regime 1, 2 and 3. Note that the field dependence of the experimental critical currents is in excellent agreement with the one associated with the IP_P/OP_P transition in the simulations. In addition no microwave power was measured in region where an IP_P mode is predicted . We believe that, most probably, the weak microwave emission associated with these IP_P mode in a WAD-STT structure is too small to be measured with our experimental setup (this point will be discussed in the section 4).

Finally, the predicted IP_{AP} precession mode in the lower left corner of the diagram characterized by a red shift regime with current and moderate precession amplitude was not observed experimentally.

3.2. Initial configuration : AP

We can go deeper into the compared analysis of experiments and simulations by looking at some additional features observed when one starts from the antiparallel AP configuration. In Fig. 5(a) and (b), we show respectively the experimental and the simulated phase diagrams for increasing current starting from *an initial AP configuration*. The experimental diagram was constructed by measuring $R(I)$ curves for different values of applied field and increasing the current starting from the high resistance AP configuration. The resistance level is plotted in colour scale in Fig. 5(a) and the corresponding $R(I)$ curves are plotted Fig. 5(c). Experimentally, starting from the AP configuration and above a positive threshold current, the magnetization switches sharply from the AP to P configuration. Then for a larger current, an increase of the resistance is observed due to the onset of a steady precession mode. This behavior is well reproduced by the macrospin simulation (see Fig. 5(b)). In particular, the critical currents associated with the magnetization switching from AP to P state are well reproduced, as well as their dependence with the applied magnetic field.

Now we compare the experimental (Fig. 5(c)) and simulated $R(I)$ (Fig. 5(d)) curves obtained for increasing current starting from an initial AP configuration. A good agreement is obtained (see for example the critical currents or the variation of resistance). In particular, the simulated increase of resistance associated with the transition from the IP_P to the OP_P state is reversible as is the case in experiments. If one calculates the differential resistance $dV/dI=R+IdR/dI$ using the simulated $R(I)$ curves, one observes that this transition is associated with a peak in the $dV/dI(I)$ curves. This reproduces the experimental observations where such peaks, that characterize the reversibility of the transition, have been always observed at the onset of microwave emission (see Ref.¹⁸). In addition, for both simulations and experiments, no significant variation of the resistance is observed for the in-plane precession IP_P mode. However, the simulation overestimates the stability of the IP_{AP} precession mode around the AP configuration at the expense of the P state (see IP_{AP} zone in Fig. 5(b) and Fig. 5(d)). This can be explained by an underestimation of the effect of temperature

caused by a sweeping ramp 10^5 faster in simulations than in experiments. With a slower current ramp, the IP_{AP} mode should be more unstable and thus the reversal toward the P state should be favored. This may also explain why we did not measure microwave power associated with this dynamical precession mode.

3.3. Frequency of the precession

We compare in Fig. 6(a) the experimental and calculated $f(I)$ curves for several values of applied field. A good agreement is obtained for fields close to the zero effective field ($H_{eff} = 2$ and 10 Oe) corresponding to the regime 1 in the phase diagram. In particular, the blue shift with current and the decrease of frequency with field observed experimentally is well reproduced by the simulation. Simulations and experiments significantly differ for higher negative field ($H_{eff} = -45$ Oe). In particular, the saturation regime (regime 2) characterized by a frequency approximately constant with current is not reproduced by the simulation. However, the experimental slope of frequency with current df/dI before saturation ($H_{eff} = -45$ Oe ($7 \text{ mA} \leq I \leq 9 \text{ mA}$), $H_{eff} = 2$ Oe and $H_{eff} = 10$ Oe) is well reproduced by the simulations. This seems to indicate that the regime before saturation (regime 1) is closer to an homogeneous precession mode than the regimes observed for higher current (regime 2 and 3).

The disagreement simulation/experiments of the $f(I)$ curve at high negative field reflects a decrease of frequency with field lower in simulations than in experiments. This appears on Fig. 6(b-c), where the experimental and simulated dependence of the frequency with magnetic field are compared for $I = 10$ and 11 mA. However, the general shape of the experimental $f(H)$ curve in the red shift regime for higher field values is qualitatively reproduced by the simulation.

4. DISCUSSION

The macrospin simulations well reproduce in overall the main experimental features: the region in current-field diagram with larger power emission and increased resistance, the frontiers between the main different static and dynamical states, and the dc resistance of these different states. This agreement is quite satisfactory if we consider the crude macrospin

approximation that was used.

The direct comparison of the experimental and simulated dynamical phase diagrams clearly suggests that the observed excitations are associated with an out-of-plane precession mode. This is confirmed by the blue shift in current and the red shift in field observed in the dynamical regime 1, signature of this dynamical mode. However, the macrospin simulation do not reproduce the saturation regimes observed at low applied field and for a large current (regime 2 and 3) (see Fig. 6(a)). In this range of parameters, we believe that these regimes are probably associated to an inhomogeneous distribution of magnetization. It is worth noting that the only two other groups who observed a blue shift regime for an in-plane applied field, did also observe this saturation (or decrease) of the frequency for larger applied current (see Fig. 3, Ref.²⁹ and Ref.³⁰), suggesting the intrinsic character of this dynamical feature. On the basis of micromagnetic simulations³⁰, it has been recently suggested that this behavior can be attributed to the onset of inhomogeneous dynamical modes characterized by a mean out-of-plane component of magnetization $\langle m_z \rangle$ lower than for the uniform mode. The onset of such non standard modes leads to a decrease of the large magnetostatic energy generated by the strong demagnetizing field when the magnetization goes out of the film plane. The frequency of precession being proportional to $\langle m_z \rangle$, the decrease of $\langle m_z \rangle$ results in a decrease of the frequency as compared to the macrospin prediction and thus explains this saturation phenomenon. The in-plane Oersted field may also play a role: in the case of an out-of-plane precession mode, it tends to pull the magnetization towards the film plane. This also leads to a decrease of the precession frequency³¹.

Another point to discuss is, as already mentioned, the non-observation of a red shift regime associated with the IP_P mode in our experiments. This regime was not observed experimentally in the Co(8 nm)/Cu/Py(8 nm) nanopillar described in this paper. However, we could observe it in a nanopillar having a different WAD-STT structure Co(4 nm)/Cu/Py(8 nm). In this nanopillar, before the onset of the higher power blue shifting microwave peaks, signals of very low amplitude presenting a clear red shift behaviour have been observed. In *standard* nanopillars, this IP_P mode corresponding to a large precession angle goes with a large emitted power^{5,32}. This difference between *standard* and WAD-STT samples can be explained by a weaker slope of the angular dependence of the GMR for angles around $\varphi = 0$ in the case of a WAD-STT³³. This results in a weak variation of the resistance (and therefore a very weak power) for in-plane oscillations of magnetization

even for large angles. In our calculations, we accounted for this specific angular dependence of the GMR by using a normalized resistance $r(\varphi) = \sin^2(\varphi/2)/(1 + \chi \cos^2(\varphi/2))$ with an asymmetry factor³³ $\chi = 7.7$. As can be seen on Fig. 3(b) or reffig4(d), this results in a low increase of resistance of the device in the IP_P mode. To evaluate the influence of the angular dependence of the GMR on the emitted power, we calculated the maximum emitted power for this IP_P mode using Eq. A1 with $\chi = 7.7$, $\chi = 2$ (measured experimentally by Urazhdin *et al.* in a *standard* structure Py(6 nm)/Cu/Py(12 nm), and $\chi = 0$) corresponding to the simple angular dependence $\Delta R = (1 - \cos \theta)/2$. The simulated power in the precession mode for $\chi = 7.7$ is about 10 times lower than for $\chi = 2$ and 25 times lower than for $\chi = 0$. If this assumption is valid, then it allows to explain that in our experimental configuration, the measured signals in this IP_P precession mode were too weak to be detected.

Finally, our simulations allow the calculation of the output power in the OP_P mode: it is about 3.9 pW/mA², should compare to the maximum measured output power of about 4.5×10^{-2} pW/mA², *i.e.* approximately a factor 80 smaller. This discrepancy may arise from several factors. First, due to the impedance mismatch and the attenuation of the signal in the high frequency line and the variation of the amplification gain with frequency, the measured signal (after taking into account the amplification) is only a fraction of the actual emitted signal. Second, the fact that the OP_P mode predicted by the macrospin simulation has been rarely observed experimentally⁵ indicates the macrospin approximation does not describe properly the dynamics in this precession mode. Recently, micromagnetic calculations by Berkov *et al.*^{34,35} have shown that this dynamical OP_P mode is sensitive to the magnetization homogeneity. Factors favoring the inhomogeneity such as temperature or the Oersted field decrease the output power in this precession mode. Third, the possible presence of ferromagnetic oxides (NiO) on the sidewalls of the pillar due to air exposure during the fabrication process³⁶ or the stronger Oersted field on the edges may force the magnetization to lie in the plane on the edges. In this case, only a part of the magnetization in the center might therefore precess in the out-of-plane direction, the resulting output power being weak.

5. CONCLUSION

As a conclusion, we have simulated the magnetization dynamics in the macrospin approximation taking into account the WAD-STT predicted for a Co(8 nm)/Cu/Py(8 nm) nanopillar by the Barnaś-Fert model^{13,18,19}. At low field, the magnetization dynamics is strongly modified as compared to a standard angular dependence of the torque. When the current is increased, at low and even zero applied field, one observes successively an in-plane precession mode (IP_P) in which frequency decreases with current ("red shift regime") and an out-of-plane precession mode (OP_P), in which the frequency increases with current ("blue shift regime"). The transition between both regimes is associated with an increase of the dc resistance and a strong increase of the output power. We have presented some experimental results that confirm this zero and low field steady precession. In the main part of the current-field phase diagram in the low field range, the frequency increases with current (blue shift regime) and decreases with field. In the remaining part of the diagram (large negative applied field and high applied current), a regime in which the frequency is approximately constant (or decreases slightly) with current is observed. The macrospin simulations reproduce the main observed experimental features (phase diagram, $R(I)$ curves, dependence of frequency with current and field) and suggest that the dynamical excitations observed experimentally are associated with an out-of-plane precession mode. However the saturation regimes observed at lower field and higher current are not reproduced by the simulation and may reveal the onset of inhomogeneous dynamical excitations. Following the first experimental confirmation¹⁸ of the STT induced zero field steady precession caused by the WAD-STT, this detailed comparison of the static and dynamical results between models and experiments and the observed general good agreement give an additional confirmation of the predicted WAD-STT by diffusive models of spin transfer. This possibility of engineering the angular dependence of the torque with different spin diffusion lengths in the magnetic layers underlines the role of the spin accumulation and the spin relaxation effects on the STT. By playing on the distribution of spin relaxation in the structure, it is therefore possible to strongly modify the STT and the magnetization dynamics induced by the torque.

6. ACKNOWLEDGEMENTS

We would like to acknowledge L. Vila for assistance in fabrication, H. Hurdequint for FMR measurements, O. Copie and B. Marcilhac for assistance in transport and frequency measurements. This work was partly supported by the French National Agency of Research ANR through the PNANO program (MAGICO PNANO-05-044-02) and the EU through the Marie Curie Training network SPINSWITCH (MRTN-CT-2006-035327).

APPENDIX A: PARAMETERS USED FOR THE MACROSPIN SIMULATION

For the macrospin simulation a gyromagnetic ratio $\gamma_0 = 2.2 \cdot 10^5$ m/(A.s) has been used. The saturation magnetization $\mu_0 M_S = 0,87$ T has been deduced from ferromagnetic resonance experiments carried out on Cu(6nm)/Py(7nm)/Cu(6nm) thin films. The anisotropy fields H_d and H_{an} can be expressed as a function of demagnetizing factor N_x , N_y et N_z associated with the shape of the nanomagnet with $H_d \approx M_s(N_z - N_y)$ et $H_{an} \approx M_s(N_y - N_x)$. If we approximate the shape of the nanomagnet with an ellipsoid with axes 150 nm, 105 nm and 8 nm, close to the lateral dimensions measured by SEM within measurement uncertainty, one obtains³⁷ $N_x=0.047$, $N_y=0.063$, $N_z=0.89$ leading to $\mu_0 H_d \approx 0.7$ T and $\mu_0 H_{an} \approx 0.014$ T. This value of H_{an} is close to the anisotropy field $\mu_0 H'_{an} \approx 0.0145$ T one can estimate from the room temperature experimental coercive field H_c ⁴⁶. For a direct comparison between experimental and theoretical phase diagrams, the uniaxial anisotropy field H_{an} was adjusted to obtain a simulated coercive field equal to the experimental one ($\mu_0 H_c = 0.009$ T). For simulation at T=0 K, we used therefore $\mu_0 H_{an} = 0.009$ T. At T=300 K and with the parameters and waiting time used in the simulation, one obtains $\mu_0 H_{an} = 0.012$ T. A Gilbert damping parameter $\alpha = 0.018$ has been used. Finally, currents are deduced from current densities using a lateral surface of the nanopillar of $A=1.38 \times 10^{-14}$ m², measured experimentally by SEM. Since the angular dependence of the GMR in a WAD-STT structure is predicted^{33,38} to deviate significantly from the commonly used dependence $\sin^2(\varphi/2)$, the normalized magnetoresistance $r = (R - R_P)/(R_{AP} - R_P)$ was calculated using the following relation^{14,15}:

$$r(\varphi) = \sin^2(\varphi/2)/(1 + \chi \cos^2(\varphi/2)) \quad (\text{A1})$$

We have used $\chi = 7.7$ that was derived experimentally by Urazhdin *et al.*³³ in a non symmetrical pillar composed of Py(6 nm)/Cu(10 nm)/Py(1.5 nm) for which a WAD-STT is also predicted.

The precession frequency was derived from the higher amplitude lowest order peak in the Fourier transform spectrum of the m_y component. In the case, very common experimentally, of a slight misalignment between the magnetization of the polarizing layer and the easy axis of the free layer, this frequency corresponds actually to the higher amplitude lowest order frequency measured experimentally^{39 47}. The output power P corresponding to the simulated trajectories is deduced from the reduced resistance r using $P/I^2 = \Delta R_{exp}^2/Z_c \cdot \langle (r - \langle r \rangle)^2 \rangle$, with $\Delta R_{exp} = R_{AP} - R_P = 51 \text{ m}\Omega$ the experimental static variation of resistance due to the GMR, and $Z_c = 50 \Omega$ the characteristic impedance of the high frequency line. $\langle \dots \rangle$ indicates the mean value of 40 ns after relaxation of the magnetization.

The LLG equation (1) has been solved using a fourth order Runger-Kutta algorithm with a time step of 1 ps. For simulation at $T=0 \text{ K}$, to let magnetization reach a stationary state, a 100 ns relaxation time has been used, then trajectories are saved over a 40 ns. These trajectories are used for the fast Fourier transform calculations and the deduction of the magnetoresistance. For simulation at $T=300 \text{ K}$, after application of the current, a relaxation time of 30 ns has been used and simulations have been carried out by sweeping current with a 10^5 mA/s ramp. The plotted frequency and resistance vs current curves are averaged over 5 realizations or more.

¹ J. C. Slonczewski, Journal of Magnetism and Magnetic Materials **159**, L1 (1996).

² L. Berger, Physical Review B **54**, 9353 (1996).

³ J. A. Katine, F. J. Albert, R. A. Buhrman, E. B. Myers, and D. C. Ralph, Physical Review Letters **84**, 3149 (2000).

⁴ J. Grollier, V. Cros, A. Hamzic, J. M. George, H. Jaffrs, A. Fert, G. Faini, J. B. Youssef, and H. Legall, Applied Physics Letters **78**, 3663 (2001).

⁵ S. I. Kiselev, J. C. Sankey, I. N. Krivorotov, N. C. Emley, R. J. Schoelkopf, R. A. Buhrman, and D. C. Ralph, Nature **425**, 380 (2003).

⁶ W. H. Rippard, M. R. Pufall, S. Kaka, S. E. Russek, and T. J. Silva, Physical Review Letters

- 92**, 027201 (2004).
- ⁷ M. D. Stiles and A. Zangwill, *Physical Review B* **66**, 014407 (2002).
- ⁸ A. Brataas, G. E. W. Bauer, and P. J. Kelly, *Physics Report* **427**, 157 (2006).
- ⁹ X. Waintal, E. B. Myers, P. W. Brouwer, and D. Ralph, *Physical Review B* **62**, 12317 (2000).
- ¹⁰ T. Valet and A. Fert, *Physical Review B* **48**, 7099 (1993).
- ¹¹ Q. Yang, P. Holody, S.-F. Lee, L. L. Henry, R. Loloee, P. A. Schroeder, W. P. P. Jr., , and J. Bass, *Physical Review Letters* **72**, 3274 (1994).
- ¹² A. Fert, V. Cros, J. M. George, J. Grollier, H. Jaffres, A. Hamzic, A. Vaures, G. Faini, J. B. Youssef, and H. Legall, *Journal of Magnetism and Magnetic Material* **272**, 1706 (2004).
- ¹³ J. Barnaś, A. Fert, M. Gmitra, I. Weymann, and V. Dugaev, *Physical Review B* **72**, 024426 (2005).
- ¹⁴ J. C. Slonczewski, *Journal of Magnetism and Magnetic Materials* **247**, 324 (2002).
- ¹⁵ A. Manchon and J. C. Slonczewski, *Physical Review B* **73**, 184419 (2006).
- ¹⁶ S. Urazhdin, N. O. Birge, J. W. P. Pratt, and J. Bass, *Applied Physics Letters* **84**, 1516 (2004).
- ¹⁷ M. AlHajDarwish, H. Kurt, S. Urazhdin, A. Fert, R. Loloee, J. W. P. Pratt, and J. Bass, *Physical Review Letters* **93**, 157203 (2004).
- ¹⁸ O. Boulle, V. Cros, J. Grollier, L. G. Pereira, C. Deranlot, F. Petroff, G. Faini, J. Barnaś, and A. Fert, *Nature Physics* **3**, 492 (2007).
- ¹⁹ J. Barnaś, A. Fert, M. Gmitra, I. Weymann, and V. Dugaev, *Materials Science and Engineering B* **126**, 271 (2006).
- ²⁰ M. Gmitra and J. Barnaś, *Physical Review Letters* **96**, 207205 (2006).
- ²¹ J. Zhang, P. M. Levy, S. Zhang, and V. Antropov, *Physical Review Letters* **93**, 256602 (2004).
- ²² W. F. Brown, *Physical Review* **130**, 1677 (1963).
- ²³ S. E. Russek, S. Kaka, W. H. Rippard, M. R. Pufall, and T. J. Silva, *Physical Review B* **71**, 104425 (2005).
- ²⁴ A. N. Slavin and P. Kabos, *Ieee Transactions On Magnetism* **41**, 1264 (2005).
- ²⁵ S. M. Rezende, F. M. de Aguiar, and A. Azevedo, *Physical Review Letters* **94**, 037202 (2005).
- ²⁶ G. Bertotti, C. Serpico, I. D. Mayergoyz, A. Magni, and M. A. R. Bonin, *Physical Review Letters* **94**, 127206 (2005).
- ²⁷ J. Z. Sun, *Physical Review B* **62**, 570 (2000).
- ²⁸ M. Stiles and J. Miltat (Elsevier, New York, 2005).

- ²⁹ S. I. Kiselev, J. C. Sankey, I. N. Krivorotov, N. C. Emley, A. G. F. Garcia, R. A. Buhrman, and D. C. Ralph, *Physical Review B* **72**, 064430 (2005).
- ³⁰ D. Houssameddine, U. Ebels, B. Dela, B. Rodmacq, I. Firastrau, F. Ponthenier, M. Brunet, C. Thirion, J.-P. Michel, L. Prejbeanu-Buda, et al., *Nature Materials* **6**, 441 (2007).
- ³¹ G. D. Loubens, Ph.D. thesis, Université Paris Sud 11, orsay (2005).
- ³² J. C. Sankey, I. N. Krivorotov, S. I. Kiselev, P. M. Braganca, N. C. Emley, R. A. Buhrman, and D. C. Ralph, *Physical Review B* **72**, 224427 (pages 5) (2005).
- ³³ S. Urazhdin, R. Loloee, and J. W. P. Pratt, *Physical Review B* **71**, 100401 (pages 4) (2005).
- ³⁴ D. V. Berkov and N. L. Gorn, *Physical Review B* **72**, 094401 (2005).
- ³⁵ I. N. Krivorotov, D. V. Berkov, N. L. Gorn, N. C. Emley, J. C. Sankey, D. C. Ralph, and R. A. Buhrman, *Physical Review B* **76**, 024418 (2007).
- ³⁶ N. C. Emley, I. N. Krivorotov, O. Ozatay, A. G. F. Garcia, J. C. Sankey, D. C. Ralph, and R. A. Buhrman, *Physical Review Letters* **96**, 247204 (2006).
- ³⁷ J. A. Osborn, *Physical Review* **67**, 351 (1945).
- ³⁸ J. Manschot, A. Brataas, and G. E. W. Bauer, *Physical Review B* **69**, 092407 (2004).
- ³⁹ B. Montigny and J. Miltat, *Journal of Applied Physics* **97**, 10C708 (2005).
- ⁴⁰ M. P. Sharrock, *IEEE Transactions on Magnetism* **26**, 193 (1990).
- ⁴¹ According to our notation, the electrons are going from the Co fixed layer to the NiFe free layer for a positive current. Note that the excitations of the parallel state by a positive current is in contrary with the standard situation in which a negative current excites the parallel state.
- ⁴² We check this decrease is not due to the different value of H_{an} used for $T=0$ K and $T=300$ K
- ⁴³ At low current below I_c^1 , the plotted frequency corresponds to small elliptical precession of magnetization induced by thermal fluctuations whose frequency (2.58 GHz) is equal to the Kittel FMR frequency (2.58 GHz). The small variation of the frequency observed at low current for the in-plane precession mode between 0 and 300 K is due to the higher anisotropy field used in the simulation for $T=300$ K ($H_{an} = 120$ Oe instead of 90 Oe.).
- ⁴⁴ This decrease appears more clearly at even lower field ($H_{eff} \leq -75$ Oe) close to the switching field (not shown).
- ⁴⁵ These frontiers were constructed by considering the dependence of the emission frequency with current at fixed field from more than a hundred microwave spectra. Similar frontiers are obtained if the phase diagram is constructed from the dependence of the emission frequency with field at

fixed current (not shown).

⁴⁶ The coercive field H_c at a temperature T can be expressed as a function of the uniaxial anisotropy field H'_{an} ⁴⁰ $H_c(H'_{an}) = H_{an}(1 - [k_B T / E_k \ln(f_0 \tau_m / \ln 2)]^{1/2})$ with $E_k = 1/2 \mu_0 M_s V H'_{an}$, f_0 the attempt frequency of the order of 1 GHz and τ_m the time measurement of the order of 1s. By solving this equation, using experimental parameters and assuming $f_0=1$ GHz, one finds $H'_{an} \approx 145$ Oe.

⁴⁷ One can note however that the frequency derived from the m_x and the m_y component are the same for an out-of-plane precession mode.

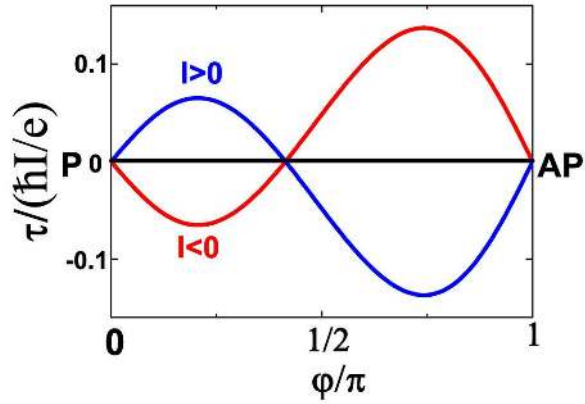


Fig1,
Boulle *et al.*

FIG. 1: Magnitude of the spin transfer torque τ on the free Py layer of a Au(infinite)/Cu(5 nm)/Py(8 nm)/Cu(10 nm)/Co(8 nm)/Ta(10 nm)/Cu(infinite) multilayer as a function of the angle φ between the magnetizations of the free Py and fixed Co layers, calculated with the Barnás-Fert model¹³ ($\tau(\varphi) = -P(\varphi) \sin \varphi I \hbar / (2e)$). Electrons flow from the Co layer to the Py layer for a positive current I .

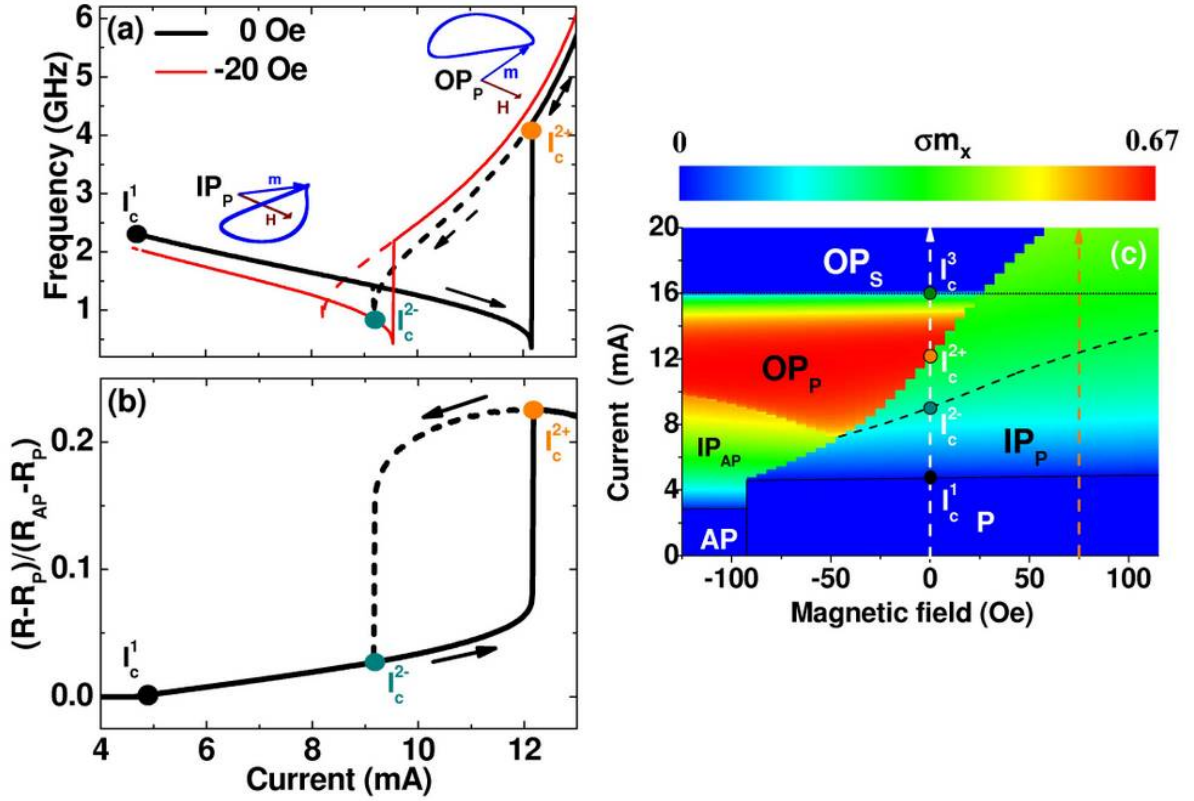


Fig. 2, Boule *et al.*

FIG. 2: $T=0$ K. (a) Frequency of precession as a function of current for several applied field for increasing (plain line) and decreasing (dashed line) current. (b) Normalized resistance as function of current for $H=0$ for increasing (plain line) and decreasing (dashed line) current. (c) Dynamical phase diagram for increasing current (σ_{mx} in color scale) and decreasing current (dashed and dotted frontiers). For decreasing current, the dotted white line corresponds to the frontier of the OP_S with the OP_P state and the dashed black line to the frontier of the OP_P state with the IP_P state. Plain black lines define the frontiers of the P and AP state. Static and dynamical states are defined in the text.

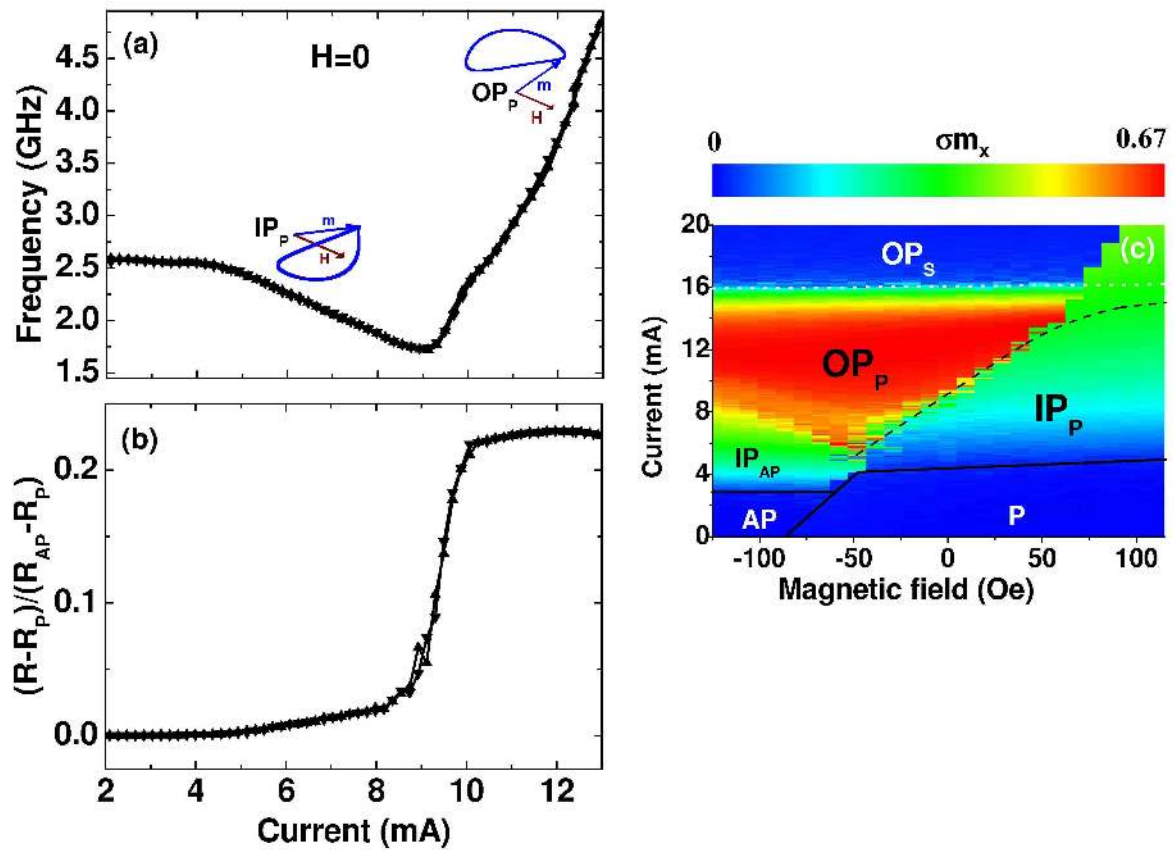


Fig. 3, Boulle *et al.*

FIG. 3: $T=300$ K. (a-b) Frequency of precession (a) and normalized resistance (b) as a function of current for increasing (upward triangles) and decreasing (downward triangles) current for $H=0$. (c) Dynamical phase diagram for increasing current (σ_{mx} in color scale) and decreasing current (dashed and dotted frontiers).

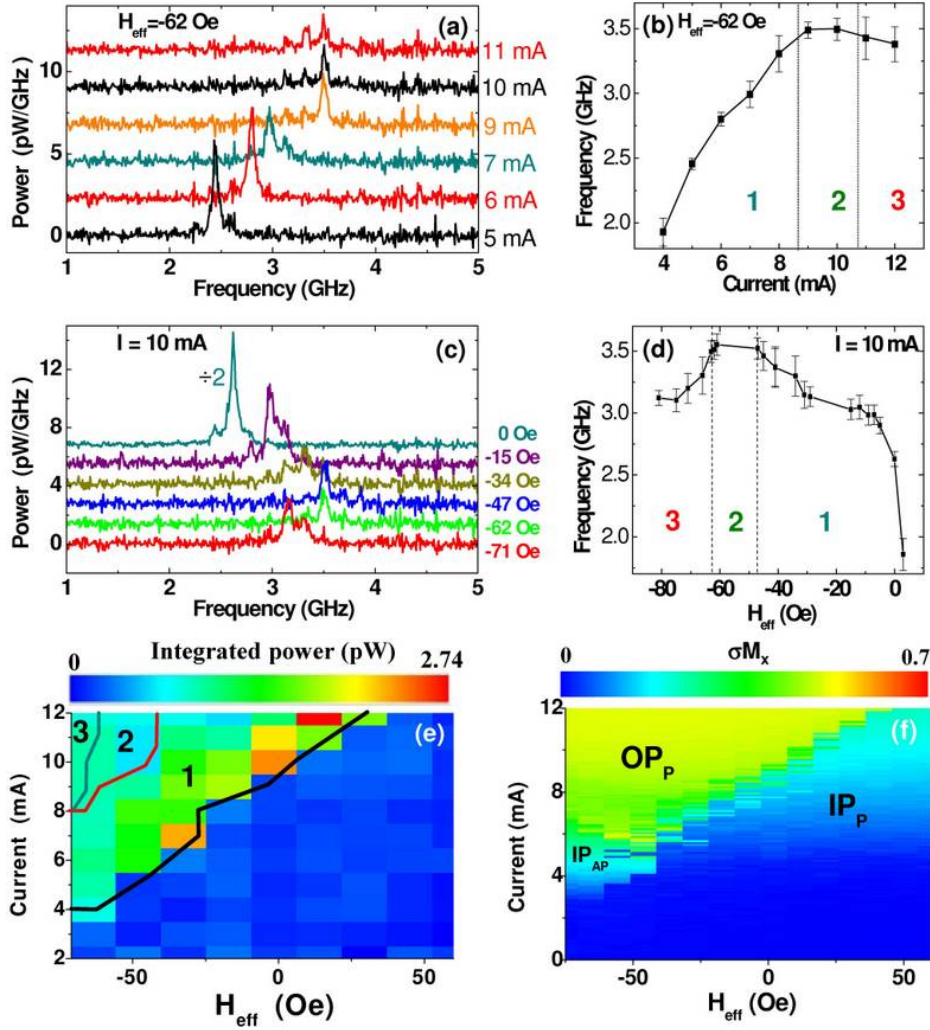


Fig. 4, Boulle *et al.*

FIG. 4: (a): Microwave power spectra for several values of injected current and $H_{eff} = -63$ Oe. (b) Frequency associated to the peaks in the microwave spectra as a function of current for $H_{eff} = -63$ Oe. (c): Microwave power spectra for several values of H_{eff} and $I=10$ mA. (d) Frequency associated to the peaks in the microwave spectra as a function of the H_{eff} for $I=10$ mA. H_{eff} is defined as $H_{eff} = H_{app} + H_{dip}$ with $H_{dip} = -43$ Oe. In (b) and (d), error bars correspond to the line width of the peak. (e) Experimental dynamical current-field phase diagram for increasing current starting from an initial P state. The microwave power is plotted in color scale. The dynamical regimes denoted as 1, 2 and 3 are defined in the text. (f) Simulated current-field phase diagram for increasing current starting from an initial P state. The amplitude of oscillation (σ_{mx}) is plotted in color scale.

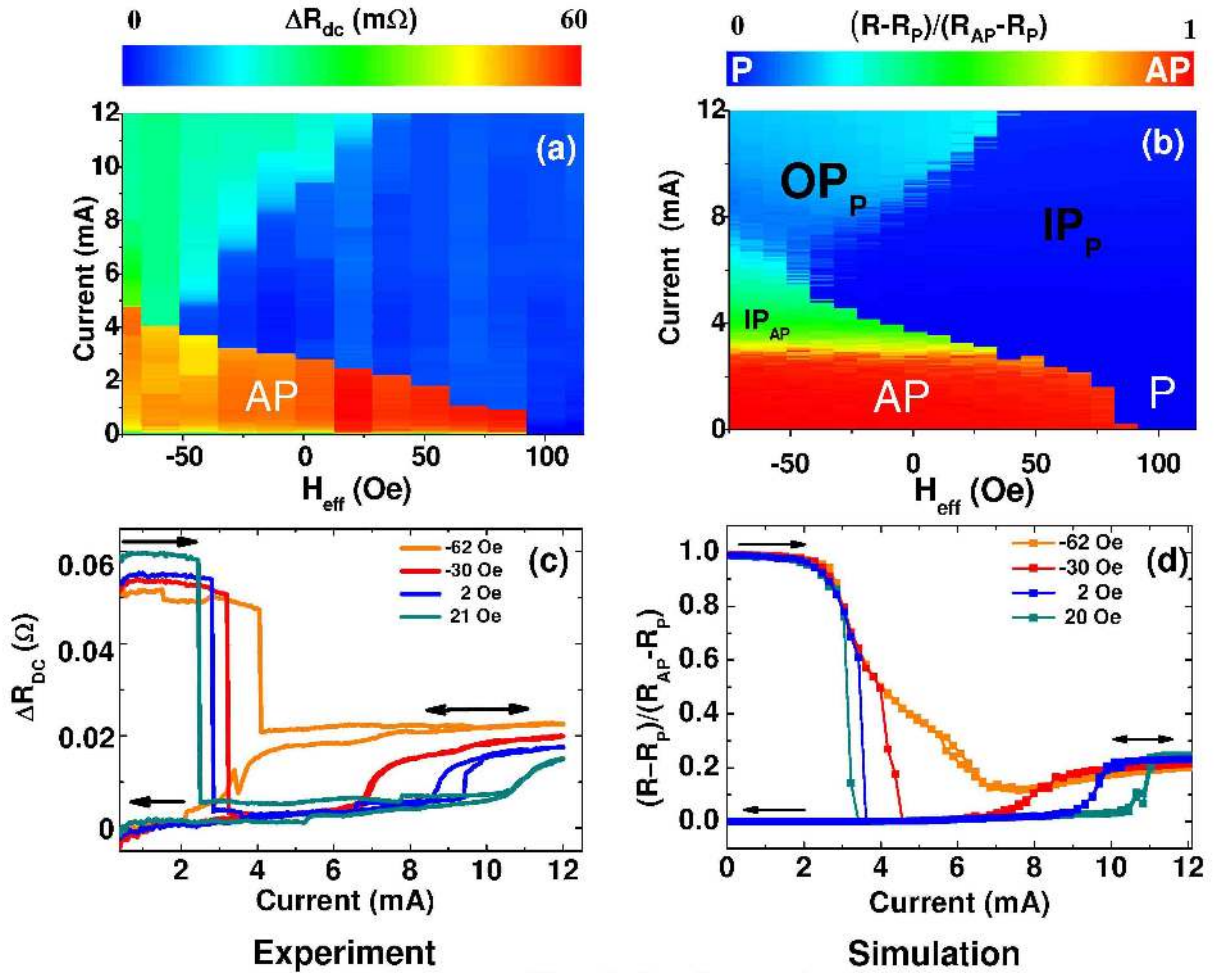


Fig. 5, Boulle *et al.*

FIG. 5: (a) Experimental phase diagram for increasing current starting from an initial *AP* state. The normalized resistance of the sample ΔR is plotted in color scale. (b) Corresponding simulated phase diagram (normalized resistance in color scale). (c): Measured resistance as a function of current for several value of H_{eff} starting from an initial *AP* state for successively increasing and decreasing current. (d): Corresponding simulated normalized resistance vs current curves. The experimental normalized resistance ΔR is obtained by subtracting from the experimental R versus I curves a reference curve to remove the changes in resistance due to Joule heating.

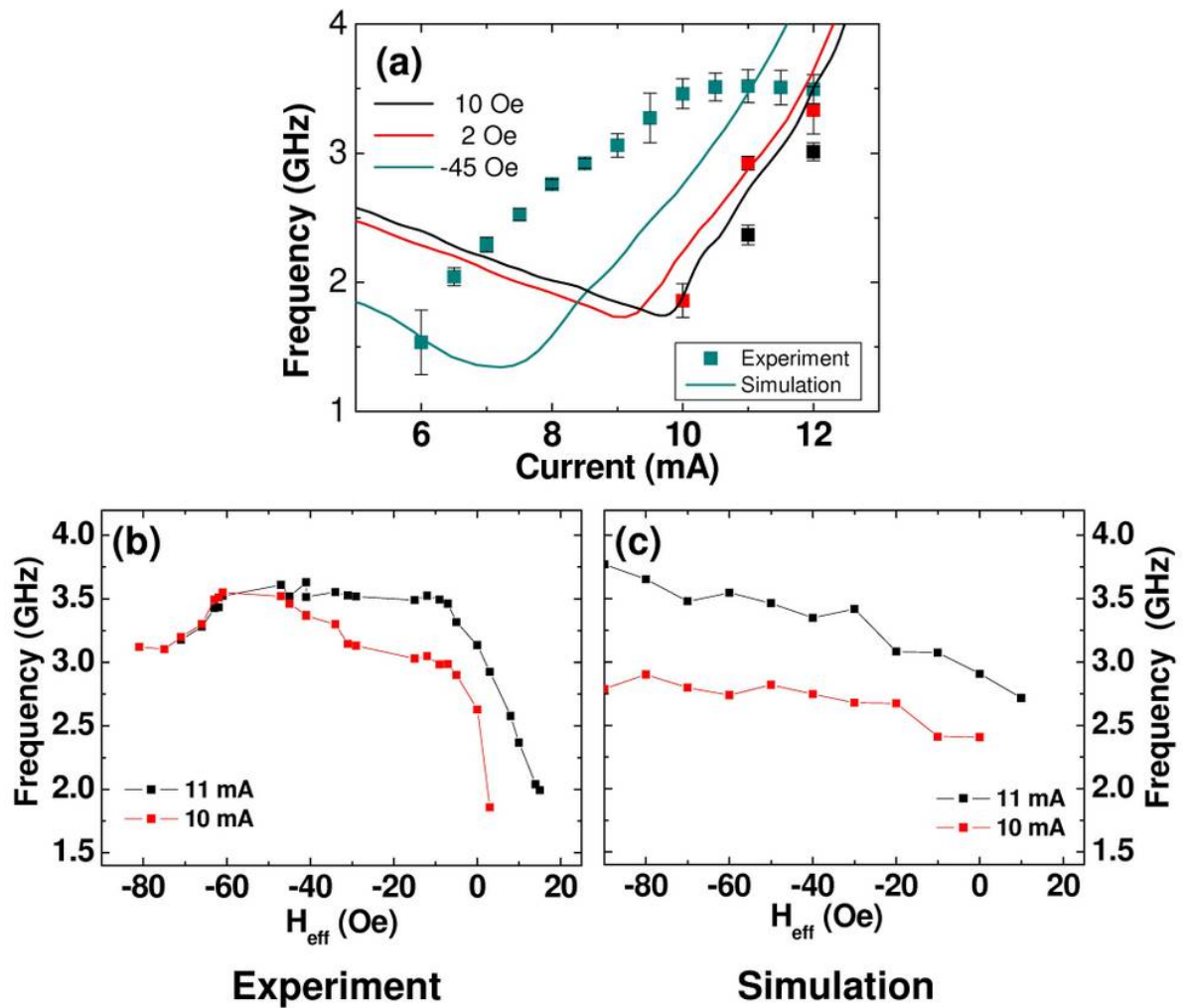


Fig. 6, Boulle *et al.*

FIG. 6: (a) Simulated (plain lines) and experimental (square points) variation of frequency with current for several values of H_{eff} . (b-c): Simulated (b) and experimental (c) variation of frequency with H_{eff} for $I=10$ mA and $I= 11$ mA.